

Endpoint-Explicit Differential Dynamic Programming via Exact Resolution

Maria Parilli[✉] Sergi Martínez[✉] Carlos Mastalli[✉]

Abstract—We introduce a novel method for handling endpoint constraints in constrained differential dynamic programming (DDP). Unlike existing approaches, our method guarantees quadratic convergence and is exact, effectively managing rank deficiencies in both endpoint and stagewise equality constraints. It is applicable to both forward and inverse dynamics formulations, making it particularly well-suited for model predictive control (MPC) applications and for accelerating optimal control (OC) solvers. We demonstrate the efficacy of our approach across a broad range of robotics problems and provide a user-friendly open-source implementation within CROCODDYL.

I. INTRODUCTION

Efficient and exact handling of endpoint constraints is a critical component for the parallelization of algorithms in optimal control (OC). In recent years, various approaches have emerged to address this challenge through endpoint constraints. One straightforward approach is leveraging algorithms for distributed optimization such as the alternating direction method of multipliers (ADMM) [1]. This approach was recently applied by Bishop et al. [2]. However, ADMM is inherently inexact and achieves only linear convergence at best, due to its reliance on augmented Lagrangian techniques (see [3, Section II-C, p. 6]).

A promising alternative for parallelizing computations is the use endpoint-explicit Riccati recursions, as proposed by Laine and Tomlin [4]. These recursions offer the potential for quadratic convergence. However, they manage endpoint constraints through pseudo-inverses [5], a process that is both computationally expensive and numerically unstable. Consequently, this approach is limited to linear-quadratic regulator (LQR) frameworks and struggles with more complex, nonlinear OC problems.

In many real-time robotics applications, strict terminal constraints must be met within tight computational time limits. In this context, differential dynamic programming (DDP) has become the preferred approach, as it leverages the Markovian structure of the problem through Riccati recursions. This results in significantly higher computational efficiency compared to traditional sparse linear solvers (e.g., MA27, MA57, MA97 [6]) commonly used in nonlinear programming (NLP). However, recent advances in constrained DDP methods (e.g., [7]–[10]) have focused mainly on stagewise constraints, often treating endpoint constraints inexactly or using penalty-based methods, which can compromise performance in tasks requiring precise endpoint constraints.

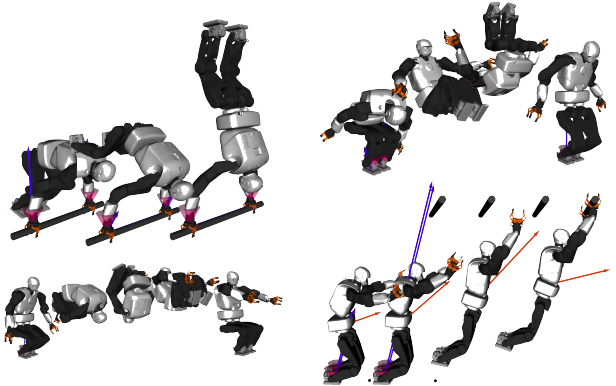


Fig. 1. Snapshots of Talos performing various gymnastic maneuvers computed using our endpoint-explicit DDP algorithm. The images show Talos executing a (top-left) handstand, (top-right) backflip, (bottom-left) frontflip, and (bottom-right) monkey bar maneuver. For each maneuver, the feet or hand placements were specified as endpoint constraints. To watch the video, click the picture or see <https://youtu.be/RBohdOhgbWw>.

A. Contribution

In this work, we address the limitation of existing methods for handling endpoint constraints in OC. Our approach is both exact and computationally efficient, offering quadratic convergence while managing rank-deficient endpoint constraints. Furthermore, it accommodates nonlinearities in both forward and inverse dynamics formulations, making it highly suitable for model predictive control (MPC) applications.

We demonstrate the effectiveness of our method across various robotics applications (Fig. 1). Our approach is adaptable to various stagewise constraints and readily accessible to practitioners through CROCODDYL [11].

II. QUADRATIC PROGRAMS WITH ENDPOINT CONSTRAINTS

Before diving into our algorithm, we first introduce a key abstraction that facilitates its development. Specifically, OC problems subject to stagewise and endpoint constraints can be locally resolved by solving the following quadratic program:

$$\begin{aligned} \min_{\mathbf{w}} \quad & \frac{1}{2} \mathbf{w}^\top \mathbf{A} \mathbf{w} - \mathbf{w}^\top \mathbf{a} \\ \text{subject to} \quad & \mathbf{B} \mathbf{w} = \mathbf{b}, \end{aligned} \tag{1}$$

at each Newton step to find the nonlinear roots that define the Karush-Kuhn-Tucker (KKT) point [12].

In this abstraction, $\mathbf{w} \in \mathbb{R}^{n_w}$ represents the primal and dual decision variables encountered in an OC problem without endpoint constraints (e.g., search direction for states, controls, and multipliers of the dynamics constraints). The matrix $\mathbf{A} \in S_{++}^{n_w}$ is a symmetric, positive definite, banded, and large,

while $\mathbf{B} \in \mathbb{R}^{n_b \times n_w}$ is the wide ($n_b \ll n_w$) Jacobian of the endpoint constraints, with $\mathbf{b} \in \mathbb{R}^{n_b}$ as its bias term.

The Lagrangian of Eq. (1) is defined as:

$$\mathcal{L}(\mathbf{w}, \mathbf{y}) = \frac{1}{2} \mathbf{w}^\top \mathbf{A} \mathbf{w} - \mathbf{w}^\top \mathbf{a} + \mathbf{y}^\top (\mathbf{B} \mathbf{w} - \mathbf{b}), \quad (2)$$

where $\mathbf{y} \in \mathbb{R}^{n_b}$ represents the Lagrange multipliers for the endpoint constraints. This allows us to establish the KKT conditions for Eq. (1) as follows

$$\begin{aligned} \nabla_{\mathbf{w}} \mathcal{L}(\mathbf{w}, \mathbf{y}) &= \mathbf{A} \mathbf{w} - \mathbf{a} + \mathbf{B}^\top \mathbf{y} = \mathbf{0}, & (\text{primal feasibility}) \\ \nabla_{\mathbf{y}} \mathcal{L}(\mathbf{w}, \mathbf{y}) &= \mathbf{B} \mathbf{w} - \mathbf{b} = \mathbf{0}, & (\text{dual feasibility}) \end{aligned} \quad (3)$$

which leads to the large symmetric saddle point system:

$$\begin{bmatrix} \mathbf{A} & \mathbf{B}^\top \\ \mathbf{B} & \mathbf{0} \end{bmatrix} \begin{bmatrix} \mathbf{w} \\ \mathbf{y} \end{bmatrix} = \begin{bmatrix} \mathbf{a} \\ \mathbf{b} \end{bmatrix} \in \mathbb{R}^{n_w + n_b}. \quad (4)$$

Numerous methodologies have been proposed in the literature for factorizing such saddle point systems. Here, we briefly overview two prominent techniques: the classical Schur-complement approach and nullspace factorization [13]. These methods are crucial due to their exactness, which is essential for ensuring fast convergence when handling endpoint constraints. This stands in contrast to inexact approaches, such as Krylov subspace method or relaxed proximal formulations [14]. The latter can be viewed as a generalized Augmented Lagrangian method [15], where convergence depends on the accuracy of the estimated multiplier \mathbf{y}_e . Moreover, solving Eq. (4) leverages second-order derivatives to achieve quadratic convergence.

A. Schur-complement resolution

Since \mathbf{A} is square and nonsingular, we can solve Eq. (4) as

$$\mathbf{y} = -\mathbf{S}^{-1}(\mathbf{b} - \mathbf{B}\mathbf{A}^{-1}\mathbf{a}), \quad (5a)$$

$$\mathbf{w} = \mathbf{A}^{-1}\mathbf{a} - \mathbf{A}^{-1}\mathbf{B}^\top \mathbf{y}, \quad (5b)$$

where $\mathbf{S} = \mathbf{B}\mathbf{A}^{-1}\mathbf{B}^\top$ denotes the Schur complement, and its inversion can be efficiently computed via a sparse Cholesky decomposition.

From Eq. (5b), we observe that the decision vector \mathbf{w} decomposes into two terms:

$$\mathbf{w} = \hat{\mathbf{w}} - \tilde{\mathbf{W}}\mathbf{y}, \quad (6)$$

where $\hat{\mathbf{w}} = \mathbf{A}^{-1}\mathbf{a}$ is the endpoint-independent solution, and $\tilde{\mathbf{W}} = \mathbf{A}^{-1}\mathbf{B}^\top \in \mathbb{R}^{n_w \times n_b}$ accounts for the effect of the endpoint multiplier \mathbf{y} , i.e., the endpoint-dependent solution.

Finally, the banded structure of \mathbf{A} , which arises in optimal control due to its Markovian nature, allows for the application of Riccati recursions when solving Eq. (5). This results in a highly efficient algorithm for solving arbitrary constraints.

B. Nullspace resolution

If \mathbf{B} is rank deficient, the Schur complement of Eq. (5) becomes non-invertible, rendering the problem ill-posed. A straightforward solution is to parameterize the decision vector \mathbf{w} into its nullspace and range. However, this strategy: (i) requires a costly nullspace decomposition due to the large and

sparse nature of \mathbf{B} , and (ii) does not exploit the structure of \mathbf{A} , preventing efficient computation of $\hat{\mathbf{w}}$ and $\tilde{\mathbf{W}}\mathbf{y}$. Instead, we propose performing a nullspace decomposition on the Lagrange multiplier \mathbf{y} . Specifically, we parameterize \mathbf{y} as:

$$\mathbf{y} = \bar{\mathbf{Z}}\mathbf{y}_{\bar{z}} + \bar{\mathbf{Y}}\mathbf{y}_{\bar{y}}, \quad (7)$$

where $\bar{\mathbf{Z}} \in \mathbb{R}^{n_b \times n_{\bar{z}}}$ represents the nullspace basis of \mathbf{S} and $\bar{\mathbf{Y}} \in \mathbb{R}^{n_b \times n_{\bar{y}}}$ denotes its orthonormal basis. This reduces Eq. (4) to the following saddle point system:

$$\begin{bmatrix} \mathbf{B}_{\bar{z}} \mathbf{A}^{-1} \mathbf{B}_{\bar{z}}^\top & \mathbf{B}_{\bar{z}} \mathbf{A}^{-1} \mathbf{B}_{\bar{y}}^\top \\ \mathbf{B}_{\bar{y}} \mathbf{A}^{-1} \mathbf{B}_{\bar{z}}^\top & \mathbf{B}_{\bar{y}} \mathbf{A}^{-1} \mathbf{B}_{\bar{y}}^\top \end{bmatrix} \begin{bmatrix} \mathbf{y}_{\bar{z}} \\ \mathbf{y}_{\bar{y}} \end{bmatrix} = - \begin{bmatrix} \mathbf{b}_{\bar{z}} - \mathbf{B}_{\bar{z}} \hat{\mathbf{w}} \\ \mathbf{b}_{\bar{y}} - \mathbf{B}_{\bar{y}} \hat{\mathbf{w}} \end{bmatrix}, \quad (8)$$

where $\mathbf{B}_{\bar{z}} \triangleq \bar{\mathbf{Z}}^\top \mathbf{B}$, $\mathbf{B}_{\bar{y}} \triangleq \bar{\mathbf{Y}}^\top \mathbf{B}$, $\mathbf{b}_{\bar{z}} \triangleq \bar{\mathbf{Z}}^\top \mathbf{b}$ and $\mathbf{b}_{\bar{y}} \triangleq \bar{\mathbf{Y}}^\top \mathbf{b}$. Additionally, since $\mathbf{B}_{\bar{z}} = \mathbf{0}$, the Lagrange multiplier is computed as:

$$\mathbf{y} = \bar{\mathbf{Y}}\mathbf{y}_{\bar{y}} = -\bar{\mathbf{Y}}(\mathbf{B}_{\bar{y}}\mathbf{A}^{-1}\mathbf{B}_{\bar{y}}^\top)^{-1}(\mathbf{b}_{\bar{y}} - \mathbf{B}_{\bar{y}}\hat{\mathbf{w}}). \quad (9)$$

This formulation effectively handles rank deficiency in \mathbf{B} , allowing for efficient resolution of the system even when the Schur complement is invertible.

III. OPTIMAL CONTROL WITH ENDPOINT CONSTRAINTS

Nonlinear OC problems with endpoint constraints can be formulated using either forward or inverse dynamics. In inverse dynamics formulation, the problem involves handling stagewise equality constraints as follows

$$\begin{aligned} \min_{\mathbf{x}_s, \mathbf{u}_s} \quad & \ell_N(\mathbf{x}_N) + \sum_{k=0}^{N-1} \ell_k(\mathbf{x}_k, \mathbf{u}_k) \\ \text{s.t.} \quad & \tilde{\mathbf{x}}_0 \ominus \mathbf{x}_0 = \mathbf{0}, & (\text{initial constraint}) \\ & \mathbf{f}_k(\mathbf{x}_k, \mathbf{u}_k) \ominus \mathbf{x}_{k+1} = \mathbf{0}, & (\text{integrator / forward dyn.}) \\ & \mathbf{h}_k(\mathbf{x}_k, \mathbf{u}_k) = \mathbf{0}, & (\text{inverse dyn.}) \\ & \mathbf{r}(\mathbf{x}_N) = \mathbf{0}. & (\text{endpoint constraint}) \end{aligned} \quad (10)$$

The state $\mathbf{x} \in \mathcal{X} \subseteq \mathbb{R}^{n_x}$ lies in a smooth manifold, with $\tilde{\mathbf{x}}_0$ specifying the system's initial state. The control inputs $\mathbf{u}_k \in \mathbb{R}^{n_u}$ is optimized to minimize the objective, where: (i) $\ell_k : \mathbb{R}^{n_x} \times \mathbb{R}^{n_u} \rightarrow \mathbb{R}_{++}$ represents the stagewise cost for each time step, (ii) $\ell_N : \mathbb{R}^{n_x} \rightarrow \mathbb{R}_{++}$ is the terminal cost, (iii) $\mathbf{f}_k : \mathbb{R}^{n_x} \times \mathbb{R}^{n_u} \rightarrow \mathbb{R}^{n_x}$ captures the system's forward dynamics or integrator as in [16], (iv) $\mathbf{h}_k : \mathbb{R}^{n_x} \times \mathbb{R}^{n_u} \rightarrow \mathbb{R}^{n_v+n_c}$ incorporates inverse dynamics and contact constraints, with n_v representing the dimension of inverse dynamics and n_c the dimension of contact constraints, (v) $\mathbf{r} : \mathbb{R}^{n_x} \rightarrow \mathbb{R}^{n_r}$ defines the endpoint constraint. Moreover, \mathbf{u} represents joint efforts in forward dynamics formulations [17] or generalized accelerations and contact forces in inverse dynamics formulations [16].

To solve this large optimization problem, we find the KKT point using an iterative routine based on the Newton method.

This approach requires factorizing the following system of equations:

$$\begin{bmatrix} -\mathbf{I} & & & & \\ -\mathbf{I} & \ddots & & & \\ & \mathcal{L}_{\mathbf{x}\mathbf{x}_k} \mathcal{L}_{\mathbf{x}\mathbf{u}_k} \mathbf{h}_{\mathbf{x}_k}^T \mathbf{f}_{\mathbf{x}_k}^T & & & \\ & \mathcal{L}_{\mathbf{u}\mathbf{x}_k} \mathcal{L}_{\mathbf{u}\mathbf{u}_k} \mathbf{h}_{\mathbf{u}_k}^T \mathbf{f}_{\mathbf{u}_k}^T & & & \\ \mathbf{h}_{\mathbf{x}_k} & \mathbf{h}_{\mathbf{u}_k} & & & \\ \mathbf{f}_{\mathbf{x}_k} & \mathbf{f}_{\mathbf{u}_k} & \ddots & & \\ & & \ell_{\mathbf{x}\mathbf{x}_N} \mathbf{r}_{\mathbf{x}_N}^T & & \\ & & \mathbf{r}_{\mathbf{x}_N} & & \end{bmatrix} \begin{bmatrix} \xi_0^+ \\ \vdots \\ \delta \mathbf{x}_k \\ \delta \mathbf{u}_k \\ \gamma_k^+ \\ \xi_{k+1}^+ \\ \vdots \\ \delta \mathbf{x}_N \\ \beta^+ \end{bmatrix} = - \begin{bmatrix} \bar{\mathbf{f}}_0 \\ \vdots \\ \ell_{\mathbf{x}_k} \\ \ell_{\mathbf{u}_k} \\ \bar{\mathbf{h}}_k \\ \bar{\mathbf{f}}_k \\ \vdots \\ \ell_{\mathbf{x}_N} \\ \bar{\mathbf{r}} \end{bmatrix} \quad (11)$$

In Eq. (11), the infeasibilities are defined as follows: $\bar{\mathbf{f}}_0 := \tilde{\mathbf{x}}_0 \ominus \mathbf{x}_0$, $\bar{\mathbf{h}}_k := \mathbf{h}_k(\mathbf{x}_k, \mathbf{u}_k)$, $\bar{\mathbf{f}}_{k+1} := \mathbf{f}_k(\mathbf{x}_k, \mathbf{u}_k) \ominus \mathbf{x}_{k+1}$, $\bar{\mathbf{r}} := \mathbf{r}(\mathbf{x}_N)$, which corresponds to initial constraint, integrator, inverse dynamics, and endpoint constraint, respectively. Moreover, ξ_0^+ , γ_k^+ , ξ_k^+ , and β^+ are their Lagrange multipliers, where the + notation stands for the next value, e.g., $\xi^+ := \xi + \delta\xi$. Additionally, \mathbf{f}_p , \mathbf{h}_p represent the Jacobians of the dynamics and constraints, ℓ_p denotes the cost gradient, where p refers to either \mathbf{x} or \mathbf{u} . The Lagrangian's Hessian, \mathcal{L}_{pp} , is introduced below.

A. Exploiting the structure of the problem

Eq. (11) matches the form introduced in Eq. (3). Specifically, we can partition Eq. (11) as follows

$$\mathbf{A} = \begin{bmatrix} -\mathbf{I} & & & & \\ -\mathbf{I} & \ddots & & & \\ & \mathcal{L}_{\mathbf{x}\mathbf{x}_k} \mathcal{L}_{\mathbf{x}\mathbf{u}_k} \mathbf{h}_{\mathbf{x}_k}^T \mathbf{f}_{\mathbf{x}_k}^T & & & \\ & \mathcal{L}_{\mathbf{u}\mathbf{x}_k} \mathcal{L}_{\mathbf{u}\mathbf{u}_k} \mathbf{h}_{\mathbf{u}_k}^T \mathbf{f}_{\mathbf{u}_k}^T & & & \\ \mathbf{h}_{\mathbf{x}_k} & \mathbf{h}_{\mathbf{u}_k} & & & \\ \mathbf{f}_{\mathbf{x}_k} & \mathbf{f}_{\mathbf{u}_k} & \ddots & & \\ & & \ell_{\mathbf{x}\mathbf{x}_N} & & \end{bmatrix}, \quad \mathbf{a} = - \begin{bmatrix} \bar{\mathbf{f}}_0 \\ \vdots \\ \ell_{\mathbf{x}_k} \\ \ell_{\mathbf{u}_k} \\ \bar{\mathbf{h}}_k \\ \bar{\mathbf{f}}_k \\ \vdots \\ \ell_{\mathbf{x}_N} \end{bmatrix}, \quad \mathbf{B} = -[\mathbf{0} \ \dots \ \mathbf{0} \ \mathbf{0} \ \mathbf{0} \ \dots \ -\mathbf{r}_{\mathbf{x}_N}], \quad \mathbf{b} = -\bar{\mathbf{r}}, \quad (12)$$

where \mathbf{A} represents the KKT matrix associated to an optimal control problem without endpoint constraints, and \mathbf{a} denotes its KKT vector.

In Section II, we initially outlined an abstract solution for this large saddle point system. Now, we continue by detailing how to compute Eq. (5), leveraging the temporal structure of the problem for computational efficiency.

B. Endpoint-independent search direction

To compute the term $\hat{\mathbf{w}} = \mathbf{A}^{-1}\mathbf{a}$, we can employ two factorization techniques: the Schur-complement and the nullspace approach. Both methods enable the design of efficient Riccati recursions. These Riccati recursions are carried out by factorizing the following system of equations backward in time:

$$\begin{bmatrix} \mathcal{L}_{\mathbf{x}\mathbf{x}} & \mathcal{L}_{\mathbf{x}\mathbf{u}} & \mathbf{h}_{\mathbf{x}}^T & \mathbf{f}_{\mathbf{x}}^T & & \\ \mathcal{L}_{\mathbf{u}\mathbf{x}} & \mathcal{L}_{\mathbf{u}\mathbf{u}} & \mathbf{h}_{\mathbf{u}}^T & \mathbf{f}_{\mathbf{u}}^T & & \\ \mathbf{h}_{\mathbf{x}} & \mathbf{h}_{\mathbf{u}} & & & & \\ \mathbf{f}_{\mathbf{x}} & \mathbf{f}_{\mathbf{u}} & & & -\mathbf{I} & \\ & & & & & \mathcal{V}'_{\mathbf{x}\mathbf{x}} \end{bmatrix} \begin{bmatrix} \delta \hat{\mathbf{x}} \\ \delta \hat{\mathbf{u}} \\ \gamma^+ \\ \hat{\xi}^+ \\ \delta \hat{\mathbf{x}}' \end{bmatrix} = - \begin{bmatrix} \ell_{\mathbf{x}} \\ \ell_{\mathbf{u}} \\ \bar{\mathbf{h}} \\ \bar{\mathbf{f}} \\ \mathbf{v}'_{\mathbf{x}} \end{bmatrix}, \quad (13)$$

where $\mathcal{V}_{\mathbf{x}\mathbf{x}_N}$ and $\mathcal{V}_{\mathbf{x}_N}$ correspond to $\ell_{\mathbf{x}\mathbf{x}_N}$ and $\ell_{\mathbf{x}_N}$, respectively. The notation $(\cdot)'$ refers to quantities at the next time step $k+1$, and (\cdot) denotes the endpoint-independent variables. In each Riccati sweep, we first condense Eq. (13) into the following system of equations

$$\begin{bmatrix} \mathbf{Q}_{\mathbf{x}\mathbf{x}} & \mathbf{Q}_{\mathbf{x}\mathbf{u}} & \mathbf{h}_{\mathbf{x}}^T \\ \mathbf{Q}_{\mathbf{u}\mathbf{x}} & \mathbf{Q}_{\mathbf{u}\mathbf{u}} & \mathbf{h}_{\mathbf{u}}^T \\ \mathbf{h}_{\mathbf{x}} & \mathbf{h}_{\mathbf{u}} & \end{bmatrix} \begin{bmatrix} \delta \hat{\mathbf{x}} \\ \delta \hat{\mathbf{u}} \\ \hat{\gamma}^+ \end{bmatrix} = - \begin{bmatrix} \mathbf{Q}_{\mathbf{x}} \\ \mathbf{Q}_{\mathbf{u}} \\ \bar{\mathbf{h}} \end{bmatrix}, \quad (14)$$

where the \mathbf{Q} 's terms are defined as follows

$$\begin{aligned} \mathbf{Q}_{\mathbf{x}\mathbf{x}} &:= \mathcal{L}_{\mathbf{x}\mathbf{x}} + \mathbf{f}_{\mathbf{x}}^T \mathcal{V}'_{\mathbf{x}\mathbf{x}} \mathbf{f}_{\mathbf{x}}, & \mathbf{Q}_{\mathbf{x}} &:= \ell_{\mathbf{x}} + \mathbf{f}_{\mathbf{x}}^T \hat{\mathcal{V}}_{\mathbf{x}}^+, \\ \mathbf{Q}_{\mathbf{x}\mathbf{u}} &:= \mathcal{L}_{\mathbf{x}\mathbf{u}} + \mathbf{f}_{\mathbf{x}}^T \mathcal{V}'_{\mathbf{x}\mathbf{u}} \mathbf{f}_{\mathbf{u}}, & \mathbf{Q}_{\mathbf{u}} &:= \ell_{\mathbf{u}} + \mathbf{f}_{\mathbf{u}}^T \hat{\mathcal{V}}_{\mathbf{x}}^+, \\ \mathbf{Q}_{\mathbf{u}\mathbf{u}} &:= \mathcal{L}_{\mathbf{u}\mathbf{u}} + \mathbf{f}_{\mathbf{u}}^T \mathcal{V}'_{\mathbf{u}\mathbf{u}} \mathbf{f}_{\mathbf{u}}, \end{aligned} \quad (15)$$

with $\mathcal{L}_{\mathbf{x}\mathbf{x}} := \ell_{\mathbf{x}\mathbf{x}} + \hat{\mathcal{V}}_{\mathbf{x}}^+ \cdot \mathbf{f}_{\mathbf{x}\mathbf{x}}$, $\mathcal{L}_{\mathbf{x}\mathbf{u}} := \ell_{\mathbf{x}\mathbf{u}} + \hat{\mathcal{V}}_{\mathbf{x}}^+ \cdot \mathbf{f}_{\mathbf{x}\mathbf{u}}$, $\mathcal{L}_{\mathbf{u}\mathbf{u}} := \ell_{\mathbf{u}\mathbf{u}} + \hat{\mathcal{V}}_{\mathbf{u}}^+ \cdot \mathbf{f}_{\mathbf{u}\mathbf{u}}$, and $\hat{\mathcal{V}}_{\mathbf{x}}^+ := \hat{\mathcal{V}}_{\mathbf{x}} + \mathcal{V}'_{\mathbf{x}\mathbf{x}} \bar{\mathbf{f}}$. Next, we compute $\delta \hat{\mathbf{u}}$ as a function of $\delta \hat{\mathbf{x}}$, transforming Eq. (14) into

$$\begin{bmatrix} \mathbf{Q}_{\mathbf{u}\mathbf{u}} & \mathbf{h}_{\mathbf{u}}^T \\ \mathbf{h}_{\mathbf{u}} & \end{bmatrix} \begin{bmatrix} \delta \hat{\mathbf{u}} \\ \hat{\gamma}^+ \end{bmatrix} = - \begin{bmatrix} \mathbf{Q}_{\mathbf{u}} + \mathbf{Q}_{\mathbf{u}\mathbf{x}} \delta \hat{\mathbf{x}} \\ \bar{\mathbf{h}} + \mathbf{h}_{\mathbf{x}} \delta \hat{\mathbf{x}} \end{bmatrix}. \quad (16)$$

By solving Eq. (16) we obtain the endpoint-independent local control policy:

$$\delta \hat{\mathbf{u}} = -\hat{\pi} - \boldsymbol{\Pi} \delta \hat{\mathbf{x}}, \quad (17)$$

where $\hat{\pi}$, $\boldsymbol{\Pi}$ are the feed-forward and feedback terms in OC problems without endpoint constraints. Finally, we update its local approximation of the value function needed for the next Riccati sweep as follows

$$\delta \hat{\mathcal{V}} = \frac{\Delta \hat{\mathcal{V}}_1 + 2\Delta \hat{\mathcal{V}}_2}{2} + \delta \hat{\mathbf{x}}^T (\hat{\mathcal{V}}_{\mathbf{x}_1} + \hat{\mathcal{V}}_{\mathbf{x}_2}) + \frac{1}{2} \delta \hat{\mathbf{x}}^T \mathcal{V}_{\mathbf{x}\mathbf{x}} \delta \hat{\mathbf{x}} \quad (18)$$

with terms computed as follows:

$$\begin{aligned} \Delta \hat{\mathcal{V}}_1 &= \hat{\pi}^T \mathbf{Q}_{\mathbf{u}\mathbf{u}} \hat{\pi}, & \Delta \hat{\mathcal{V}}_2 &= -\hat{\pi}^T \mathbf{Q}_{\mathbf{u}}, \\ \hat{\mathcal{V}}_{\mathbf{x}_1} &= \boldsymbol{\Pi}^T \mathbf{Q}_{\mathbf{u}\mathbf{u}} \hat{\pi} - \mathbf{Q}_{\mathbf{x}\mathbf{u}} \hat{\pi}, & \hat{\mathcal{V}}_{\mathbf{x}_2} &= \mathbf{Q}_{\mathbf{x}} - \boldsymbol{\Pi}^T \mathbf{Q}_{\mathbf{u}}, \\ \mathcal{V}_{\mathbf{x}\mathbf{x}} &= \mathbf{Q}_{\mathbf{x}\mathbf{x}} - 2\mathbf{Q}_{\mathbf{x}\mathbf{u}} \boldsymbol{\Pi} + \boldsymbol{\Pi}^T \mathbf{Q}_{\mathbf{u}\mathbf{u}} \boldsymbol{\Pi}. \end{aligned} \quad (19)$$

For forward dynamics, Eq. (19) simplifies, where $\Delta \hat{\mathcal{V}}_1 = \hat{\pi}^T \mathbf{Q}_{\mathbf{u}}$, $\hat{\mathcal{V}}_{\mathbf{x}_1} = \mathbf{0}$, and $\mathcal{V}_{\mathbf{x}\mathbf{x}} = \mathbf{Q}_{\mathbf{x}\mathbf{x}} - \mathbf{Q}_{\mathbf{x}\mathbf{u}} \boldsymbol{\Pi}$. The expressions for $\hat{\pi}$ and $\boldsymbol{\Pi}$ in Eq. (17) vary depending on whether a forward or inverse dynamics formulation is used.

1) *Forward dynamics:* In forward dynamics formulations, where stagewise constraints $\mathbf{h}(\mathbf{x}, \mathbf{u})$ are often not considered, Eq. (16) reduces to the classical DDP algorithm, i.e.,

$$\hat{\pi}_u := \mathbf{Q}_{\mathbf{u}\mathbf{u}}^{-1} \mathbf{Q}_{\mathbf{u}} \quad \text{and} \quad \boldsymbol{\Pi}_u := \mathbf{Q}_{\mathbf{u}\mathbf{u}}^{-1} \mathbf{Q}_{\mathbf{u}\mathbf{x}}. \quad (20)$$

2) *Inverse dynamics:* In inverse dynamics formulations, when factorizing Eq. (17) using the Schur complement, the feed-forward and feedback terms are computed as follows:

$$\hat{\pi}_s := \mathbf{k} + (\mathbf{k}_s^T \tilde{\mathbf{Q}}_{\mathbf{u}\mathbf{u}} \boldsymbol{\Psi}_s^T)^T \quad \text{and} \quad \boldsymbol{\Pi}_s := \mathbf{K} + (\mathbf{K}_s^T \tilde{\mathbf{Q}}_{\mathbf{u}\mathbf{u}} \boldsymbol{\Psi}_s^T)^T \quad (21)$$

with $\mathbf{k} \triangleq \mathbf{Q}_{\mathbf{u}\mathbf{u}}^{-1} \mathbf{Q}_{\mathbf{u}}$, $\mathbf{K} \triangleq \mathbf{Q}_{\mathbf{u}\mathbf{u}}^{-1} \mathbf{Q}_{\mathbf{u}\mathbf{x}}$, $\mathbf{k}_s \triangleq \bar{\mathbf{h}} - \mathbf{h}_{\mathbf{u}} \mathbf{k}$, $\boldsymbol{\Psi}_s \triangleq \mathbf{Q}_{\mathbf{u}\mathbf{u}}^{-1} \mathbf{h}_{\mathbf{u}}^T$, $\tilde{\mathbf{Q}}_{\mathbf{u}\mathbf{u}} \triangleq (\mathbf{h}_{\mathbf{u}} \mathbf{Q}_{\mathbf{u}\mathbf{u}}^{-1} \mathbf{h}_{\mathbf{u}}^T)^{-1}$, and $\mathbf{K}_s \triangleq \mathbf{h}_{\mathbf{x}} - \mathbf{h}_{\mathbf{u}} \mathbf{K}$. Alternatively, a nullspace parametrization of $\delta \hat{\mathbf{u}}$ can handle rank deficiencies in $\mathbf{h}_{\mathbf{u}}$ both exactly and efficiently. This

approach is advantageous because it allows for parallelized computations, as detailed in [16]. Its resulting feed-forward and feedback terms are given by:

$$\hat{\pi}_n := \mathbf{Z}\mathbf{k}_n + \tilde{\mathbf{Q}}_{zz}\Psi_n\bar{\mathbf{h}} \quad \text{and} \quad \Pi_n = \mathbf{Z}\mathbf{K}_n + \tilde{\mathbf{Q}}_{zz}\Psi_n\mathbf{h}_x \quad (22)$$

where $\mathbf{Z} \in \mathbb{R}^{n_u \times n_z}$ represents the nullspace basis of \mathbf{h}_u , and $\mathbf{Y} \in \mathbb{R}^{n_u \times n_Y}$ denotes its orthonormal basis, $\mathbf{k}_n \triangleq \mathbf{Q}_{zz}^{-1}\mathbf{Q}_{zz}$, $\tilde{\mathbf{Q}}_{zz} \triangleq \mathbf{I} - \mathbf{Z}\mathbf{Q}_{zz}^{-1}\mathbf{Q}_{zu}$, $\mathbf{K}_n \triangleq \mathbf{Q}_{zz}^{-1}\mathbf{Q}_{zx}$, and $\Psi_n \triangleq \mathbf{Y}\mathbf{h}_y^{-1}$.

This nullspace approach performs three decompositions for \mathbf{Q}_{zz}^{-1} , $(\mathbf{h}_u\mathbf{Y})^{-1}$, and $[\mathbf{Y} \ \mathbf{Z}]$. These decompositions can be performed in parallel via efficient Cholesky and rank-revealing decompositions such as lower-upper (LU) and QR [18]. This makes nullspace methods an attractive alternative to inexact methods.

To compute the $\delta\hat{\mathbf{x}}_k$ terms—i.e., the remaining “primal variables” in $\hat{\mathbf{w}}$ —we perform a linear rollout as follows:

$$\delta\hat{\mathbf{x}}_{k+1} = \mathbf{f}_{\mathbf{x}_k}\delta\hat{\mathbf{x}}_k + \mathbf{f}_{\mathbf{u}_k}\delta\hat{\mathbf{u}}_k + \bar{\mathbf{f}}_{k+1} \quad \text{with} \quad \delta\hat{\mathbf{x}}_0 = \bar{\mathbf{f}}_0, \quad (23)$$

where $\delta\hat{\mathbf{u}}_k$ defined as in Eq. (17), and this equation holds $\forall k = \{0, \dots, N\}$. Algorithm 1 summarizes the procedure for computing the endpoint-independent search direction.

C. Endpoint-dependent search direction

By leveraging the previously computed Riccati recursion, we can obtain the term $\check{\mathbf{W}} = \mathbf{A}^{-1}\mathbf{B}^\top$ efficiently. This result stands from the following observations: (i) the Riccati recursion for $\check{\mathbf{w}} = \mathbf{A}^{-1}\mathbf{a}$ partially factorizes the KKT system of equations, (ii) this procedure exploits the Markovian structure inherent in optimal control problems, and (iii) we can reuse the decomposition of the KKT matrix in Eq. (16) to compute $\mathbf{A}^{-1}\mathbf{B}^\top$. To implement this, we replace

$$\begin{aligned} \mathbf{a} &= -[\bar{\mathbf{f}}_0 \ \dots \ \ell_{\mathbf{x}_k} \ \ell_{\mathbf{u}_k} \ \bar{\mathbf{h}}_k \ \bar{\mathbf{f}}_k \ \dots \ \ell_{\mathbf{x}_N}]^\top \quad \text{by} \\ \mathbf{B}^\top &= -[\mathbf{0}^\top \ \dots \ \mathbf{0}^\top \ \mathbf{0}^\top \ \mathbf{0}^\top \ \dots \ -\mathbf{r}_{\mathbf{x}_N}^\top]^\top. \end{aligned} \quad (24)$$

This implies initializing the new Riccati recursion with $-\mathbf{r}_{\mathbf{x}_N}^\top$ and solving the following system of equations:

$$\begin{bmatrix} \mathbf{Q}_{xx} & \mathbf{Q}_{xu} & \mathbf{h}_x^\top \\ \mathbf{Q}_{ux} & \mathbf{Q}_{uu} & \mathbf{h}_u^\top \\ \mathbf{h}_x & \mathbf{h}_u & \end{bmatrix} \begin{bmatrix} \delta\check{\mathbf{X}}_c \\ \delta\check{\mathbf{U}}_c \\ \delta\check{\Lambda}_c \end{bmatrix} = - \begin{bmatrix} \mathbf{Q}_{xc} \\ \mathbf{Q}_{uc} \\ \mathbf{0} \end{bmatrix}, \quad (25)$$

where $\mathbf{Q}_{xc} = \mathbf{f}_{\mathbf{x}}^\top \check{\mathcal{V}}_{\mathbf{xc}} \in \mathbb{R}^{n_x \times n_r}$, $\mathbf{Q}_{uc} = \mathbf{f}_{\mathbf{u}}^\top \check{\mathcal{V}}_{\mathbf{xc}} \in \mathbb{R}^{n_u \times n_r}$ as the “Jacobians” of the quality function associated with the endpoint-dependent search direction, and the terms $\delta\check{\mathbf{X}}_c \in$

Algorithm 1: Endpoint-Independent Search Direction

- 1 terminal value function: $\mathcal{V}_{\mathbf{xx}_N}, \check{\mathcal{V}}_{\mathbf{xc}_N} = \ell_{\mathbf{xx}_N}, \ell_{\mathbf{xc}_N}$
 - 2 **for** $k \leftarrow N - 1$ **to** 0 **do**
 - 3 | compute quality function \mathbf{Q} 's Eq. (15)
 - 4 | compute policy $\hat{\pi}$, Π Eqs. (20) to (22)
 - 5 | compute value function $\hat{\mathcal{V}}_{\mathbf{x}}, \mathcal{V}_{\mathbf{xx}}$ Eq. (18)
 - 6 compute $\delta\hat{\mathbf{x}}, \delta\hat{\mathbf{u}}$ via linear rollout Eq. (23)
-

$\mathbb{R}^{n_x \times n_r}$, $\delta\check{\mathbf{U}}_c \in \mathbb{R}^{n_u \times n_r}$, and $\delta\check{\Lambda}_c \in \mathbb{R}^{n_r \times n_r}$ denote the “primal and dual search directions”, respectively.

To exploit the problem's Markovian structure, we compute $\delta\check{\mathbf{U}}_c$ as a function of $\delta\check{\mathbf{X}}_c$. This step requires solving the following condensed system:

$$\begin{bmatrix} \mathbf{Q}_{uu} & \mathbf{h}_u^\top \\ \mathbf{h}_u & \end{bmatrix} \begin{bmatrix} \delta\check{\mathbf{U}}_c \\ \delta\check{\Lambda}_c \end{bmatrix} = - \begin{bmatrix} \mathbf{Q}_{uc} + \mathbf{Q}_{ux}\delta\check{\mathbf{X}}_c \\ \mathbf{h}_x\delta\check{\mathbf{X}}_c \end{bmatrix} \in \mathbb{R}^{(n_u+n_r) \times 2n_r}, \quad (26)$$

which, for inverse dynamics, this system can be reduced to

$$\begin{bmatrix} \mathbf{Q}_{zz} & \mathbf{Q}_{zy} \\ \mathbf{h}_y & \end{bmatrix} \begin{bmatrix} \delta\check{\mathbf{U}}_{zc} \\ \delta\check{\mathbf{U}}_{yc} \end{bmatrix} = - \begin{bmatrix} \mathbf{Q}_{zc} + \mathbf{Q}_{zx}\delta\check{\mathbf{X}}_c \\ \mathbf{h}_x\delta\check{\mathbf{X}}_c \end{bmatrix} \in \mathbb{R}^{(n_z+n_r) \times 2n_r}, \quad (27)$$

where $\mathbf{Q}_{zz} \triangleq \mathbf{Z}^\top \mathbf{Q}_{uu} \mathbf{Z}$, $\mathbf{Q}_{zy} \triangleq \mathbf{Z}^\top \mathbf{Q}_{uu} \mathbf{Y}$, $\mathbf{Q}_{zc} \triangleq \mathbf{Z}^\top \mathbf{Q}_{uc}$, $\mathbf{Q}_{zx} \triangleq \mathbf{Z}^\top \mathbf{Q}_{ux}$, $\mathbf{h}_y \triangleq \mathbf{h}_u \mathbf{Y}$, and $\delta\check{\mathbf{U}}_{zc}$, $\delta\check{\mathbf{U}}_{yc}$ are endpoint-dependent control policies parameterized in the null and range basis $[\mathbf{Y} \ \mathbf{Z}]$ obtained in Eq. (22).

Both Eqs. (26) and (27) allows us to compute an endpoint-dependent local policy of the form

$$\delta\check{\mathbf{U}}_c = -\check{\pi}_c - \Pi\delta\check{\mathbf{X}}_c, \quad (28)$$

which Π is the same term computed in Eq. (17).

1) *Forward dynamics*: In the absence of stagewise constraints $\mathbf{h}(\mathbf{x}, \mathbf{u})$, the feed-forward term for the endpoint-dependent control policy simplifies to:

$$\check{\pi}_{c_u} := \mathbf{Q}_{uu}^{-1}\mathbf{Q}_{uc}. \quad (29)$$

This simplification mirrors the result obtained in Section III-B1.

2) *Inverse dynamics*: For inverse dynamics formulations, solving Eq. (26) or (27) provides two methods for computing the feed-forward terms. These methods are:

$$\check{\pi}_{c_s} := \mathbf{k}_c + (\mathbf{k}_{sc}^\top \tilde{\mathbf{Q}}_{uu} \Psi_s^\top)^\top, \quad (\text{Schur complement}) \quad (30)$$

$$\check{\pi}_{c_n} := \mathbf{Z}\mathbf{k}_{nc}, \quad (\text{nullspace}) \quad (31)$$

where $\mathbf{k}_c \triangleq \mathbf{Q}_{uu}^{-1}\mathbf{Q}_{uc}$, $\mathbf{k}_{sc} \triangleq -\mathbf{h}_u \mathbf{k}_c$, and $\mathbf{k}_{nc} \triangleq \mathbf{Q}_{zz}^{-1}\mathbf{Q}_{zc}$.

We update the bias and “Jacobians” terms of the value function only as they are affected by replacing \mathbf{a} with \mathbf{B}^\top and we assume that $\mathbf{f}_{\mathbf{xx}} = \mathbf{f}_{\mathbf{xu}} = \mathbf{f}_{\mathbf{uu}} = \mathbf{0}$. These updates are

$$\delta\check{\mathcal{V}}_c = \frac{\Delta\check{\mathcal{V}}_{c_1} + 2\Delta\check{\mathcal{V}}_{c_2}}{2} + \delta\check{\mathbf{X}}_c^\top (\check{\mathcal{V}}_{xc_1} + \check{\mathcal{V}}_{xc_2}) + \frac{1}{2}\delta\check{\mathbf{X}}_c^\top \mathcal{V}_{xx}\delta\check{\mathbf{X}}_c \quad (32)$$

Algorithm 2: Endpoint-Dependent Search Direction

- 1 terminal value term: $\mathcal{V}_{\mathbf{xc}_N} = -\mathbf{r}_{\mathbf{x}_N}^\top$
 - 2 **for** $k \leftarrow N - 1$ **to** 0 **do**
 - 3 | compute quality terms $\mathbf{Q}_{xc}, \mathbf{Q}_{uc}$ Eq. (25)
 - 4 | compute feed-forward term $\check{\pi}_c$ Eqs. (29) to (31)
 - 5 | compute value term $\check{\mathcal{V}}_{\mathbf{xc}}$ Eq. (32)
 - 6 compute $\delta\check{\mathbf{X}}_c, \delta\check{\mathbf{U}}_c$ via linear rollout Eq. (34)
-

Algorithm 3: Compute Direction

- 1 compute endpoint-independent direction Algorithm 1
 - 2 compute endpoint-dependent direction Algorithm 2
 - 3 compute endpoint multiplier β^+ Eqs. (36) and (37)
 - 4 **for** $k \leftarrow 0$ **to** N **do in parallel**
 - 5 | compute $\delta\mathbf{x}'$ and $\delta\mathbf{u}$ Eq. (38)
 - 6 | compute $\Delta\mathcal{V}$ and $\mathcal{V}_{\mathbf{x}}$ Eq. (40)
-

with terms computed as follows:

$$\begin{aligned}\Delta\check{\mathcal{V}}_{\mathbf{c}_1} &= \check{\pi}_{\mathbf{c}}^\top \mathbf{Q}_{\mathbf{uu}} \check{\pi}_{\mathbf{c}}, \quad \check{\mathcal{V}}_{\mathbf{x}\mathbf{c}_1} = \Pi^\top \mathbf{Q}_{\mathbf{uu}} \check{\pi}_{\mathbf{c}} - \mathbf{Q}_{\mathbf{xu}} \check{\pi}_{\mathbf{c}}, \\ \Delta\check{\mathcal{V}}_{\mathbf{c}_2} &= -\check{\pi}_{\mathbf{c}}^\top \mathbf{Q}_{\mathbf{uc}}, \quad \check{\mathcal{V}}_{\mathbf{x}\mathbf{c}_2} = \mathbf{Q}_{\mathbf{xc}} - \Pi^\top \mathbf{Q}_{\mathbf{uc}}.\end{aligned}\quad (33)$$

For optimal control problems without stagewise constraints, these expressions simplify to $\Delta\mathcal{V}_{\mathbf{c}_1} = \check{\pi}_{\mathbf{c}}^\top \mathbf{Q}_{\mathbf{uc}}$, $\mathcal{V}_{\mathbf{x}\mathbf{c}_1} = \mathbf{0}$.

Finally, we compute the $\delta\check{\mathbf{X}}_{\mathbf{c}}$ terms via a linear rollout:

$$\delta\check{\mathbf{X}}'_{\mathbf{c}} = \mathbf{f}_{\mathbf{x}} \delta\check{\mathbf{X}}_{\mathbf{c}} + \mathbf{f}_{\mathbf{u}} \delta\check{\mathbf{U}}_{\mathbf{c}}, \quad \text{with } \delta\check{\mathbf{X}}_{\mathbf{c}_0} = \mathbf{0}, \quad (34)$$

which provides the remaining “primal variables” in $\check{\mathbf{W}} = \mathbf{A}^{-1}\mathbf{B}^\top$. Algorithm 2 summarizes the procedure needed to compute the endpoint-dependent search direction.

D. Endpoint multiplier and update direction

From Eq. (5a), we compute the Lagrange multiplier of the endpoint constraint β^+ efficiently by noting that

$$\mathbf{B}\mathbf{A}^{-1}\mathbf{B}^\top = \mathbf{r}_{\mathbf{x}_N} \delta\check{\mathbf{X}}_{\mathbf{c}_N}, \quad \mathbf{B}\mathbf{A}^{-1}\mathbf{a} = \mathbf{r}_{\mathbf{x}_N} \delta\hat{\mathbf{x}}_N, \quad (35)$$

because \mathbf{B} acts as a selection matrix, $\mathbf{y} = \beta^+$, and $\mathbf{b} = -\bar{\mathbf{r}}$. Thus, the multiplier is calculated as

$$\beta^+ = (\mathbf{r}_{\mathbf{x}_N} \delta\check{\mathbf{X}}_{\mathbf{c}_N})^{-1}(\bar{\mathbf{r}} + \mathbf{r}_{\mathbf{x}_N} \delta\hat{\mathbf{x}}_N). \quad (36)$$

Alternatively, to handle rank deficiencies in $\mathbf{r}_{\mathbf{x}_N}$, the endpoint multiplier can be computed via Eq. (9). This leads to

$$\beta^+ = \bar{\mathbf{Y}}_{\mathbf{c}}^\top (\bar{\mathbf{Y}}_{\mathbf{c}}^\top \mathbf{r}_{\mathbf{x}_N} \delta\check{\mathbf{X}}_{\mathbf{c}_N} \bar{\mathbf{Y}}_{\mathbf{c}})^{-1} \bar{\mathbf{Y}}_{\mathbf{c}}^\top (\bar{\mathbf{r}} + \mathbf{r}_{\mathbf{x}_N} \delta\hat{\mathbf{x}}_N), \quad (37)$$

where $\bar{\mathbf{Z}}_{\mathbf{c}} \in \mathbb{R}^{nr \times n\bar{z}_c}$ is the nullspace basis of $\mathbf{r}_{\mathbf{x}_N} \delta\check{\mathbf{X}}_{\mathbf{c}_N}$ and $\bar{\mathbf{Y}}_{\mathbf{c}} \in \mathbb{R}^{nr \times n\bar{y}_c}$ is chosen such that $[\bar{\mathbf{Z}}_{\mathbf{c}} \ \bar{\mathbf{Y}}_{\mathbf{c}}]$ spans \mathbb{R}^{nr} .

Once β^+ is computed from either Eq. (36) or (37), we update the search direction $\forall k = \{0, \dots, N\}$ as follows

$$\delta\mathbf{u} = \delta\hat{\mathbf{u}} - \delta\check{\mathbf{U}}_{\mathbf{c}} \beta^+, \quad \delta\mathbf{x}' = \delta\hat{\mathbf{x}}' - \delta\check{\mathbf{X}}_{\mathbf{c}}' \beta^+. \quad (38)$$

Moreover, the total value function is obtained by combining both Riccati passes, i.e.,

$$\delta\mathcal{V} = \frac{\Delta\mathcal{V}_1 + 2\Delta\mathcal{V}_2}{2} + \delta\mathbf{x}^\top (\mathcal{V}_{\mathbf{x}_1} + \mathcal{V}_{\mathbf{x}_2}) + \frac{1}{2} \delta\mathbf{x}^\top \mathcal{V}_{\mathbf{xx}} \delta\mathbf{x} \quad (39)$$

with $\Delta\mathcal{V}_{1,2} = \Delta\hat{\mathcal{V}}_{1,2} + \beta^{+\top} \Delta\check{\mathcal{V}}_{1,2} \beta^+$, and

$$\mathcal{V}_{\mathbf{x}_1, \mathbf{x}_2} = \check{\mathcal{V}}_{\mathbf{x}_1, \mathbf{x}_2} + \beta^{+\top} \check{\mathcal{V}}_{\mathbf{x}_1, \mathbf{x}_2} \beta^+. \quad (40)$$

Algorithm 3 summarizes the procedure to compute the total search direction.

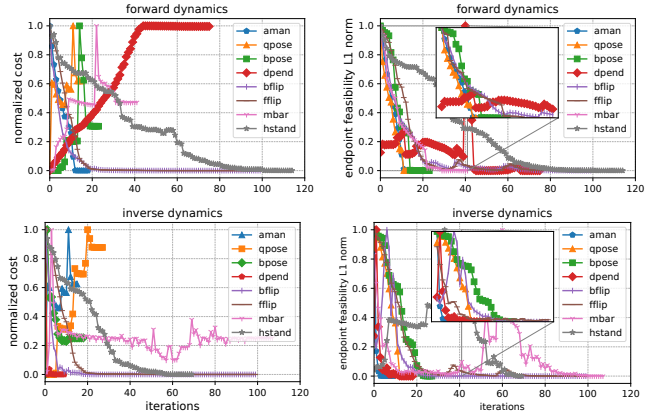


Fig. 2. Cost and endpoint feasibility evolution for forward and inverse dynamics formulations: (left) normalized cost, and (right) ℓ_1 -norm feasibility.

E. Expected improvement, merit function, and rollouts

For single-shooting rollouts, as proposed in [19], we use Eq. (39) to compute the expected improvement. However, for feasibility-driven and multiple-shooting rollouts, we adopt a quadratic approximation of the cost function, as detailed in [20, Eq. (18)] and discussed in [11].

These rollouts are essential for performing line search procedures. To accept a given step length α during this process, we employ a merit function and update its penalty parameter ν as in [16]. Our algorithm incorporates Levenberg-Marquardt regularization to enhance robustness, as in [21]. For further details on the rollouts, our merit function, and their implementation, refer to [11], [20], [22] and [16].

IV. RESULTS

We validated our endpoint-explicit DDP algorithm numerically across various robotics systems (Sections IV-A to IV-C), removing running costs for path-following (keeping regularization terms only), as our method ensures precise endpoint satisfaction. We evaluated: (i) aerial manipulation (aman), where the Borinot UAV reaches a target with its arm, (ii) legged control, with the ANYmal quadruped (qpose) or Talos biped (bpose) moving toward a CoM target, (iii) unstable equilibrium, where a double pendulum stabilizes at its upright position (dpend), and (iv) gymnastics maneuvers, where the Talos humanoid performs a backflip (bflip), frontflip (fflip), handstand (hstand), and monkey bar (mbar) to specific feet or hand poses. All tests were conducted on a MacBook Pro @ Apple M2 Pro.

A. Costs and endpoint feasibility

To validate the effectiveness of our endpoint-explicit strategy across optimal control problems with varying stagewise constraints, we compared the cost and endpoint feasibility between forward and inverse dynamics formulations. In Fig. 2, we show the normalized cost and the ℓ_1 -norm of endpoint constraint feasibility over iterations. The results show that both cost and feasibility evolution are problem-specific. As expected, the inverse dynamics formulation achieved faster convergence due to its ability to distribute nonlinearities more

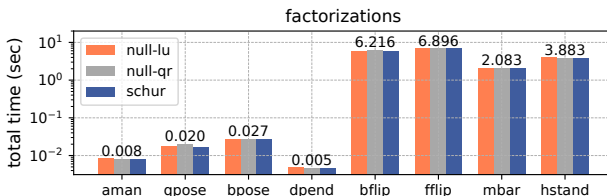


Fig. 3. Average computation time for solving different factorizations and robotics problems over 10 trials, minimum time at the top.

effectively throughout the optimization [16], [23]. Additionally, our nonmonotone Armijo-like condition allowed the algorithm to trade off between reducing endpoint infeasibility (e.g., `dpend`) and reducing cost (e.g., `mbar`).

B. Endpoint factorization

Our nullspace factorization (Section II-B) effectively handles rank deficiencies in $\mathbf{r}_{\mathbf{x}_N}$ while maintaining computational efficiency comparable to the traditional Schur complement method (Section II-A). To evaluate this, we compared computation times between the Schur complement (`schur`) and nullspace factorizations, using LU with full pivoting (`null-lu`) and QR with column pivoting (`null-qr`). Fig. 3 shows the average computation time for forward dynamics formulations initialized with the same warm start. Notably, the computational complexity remained consistent across problem sizes, from $n_x + n_u = 3$ to 108, unlike in [16], where the Riccati parallelization impacted performance. Therefore, the key advantage of applying our nullspace resolution is the ability to handle a broader class of problems without affecting the computational cost.

C. Convergence

Evaluating convergence from random cold starts allowed us to assess our algorithm's convergence properties and demonstrate its robustness and applicability. We conducted 10 trials with random initialization of \mathbf{x}_s and \mathbf{u}_s for both forward and inverse dynamics formulations. The results, including the average number of iterations to achieve convergence, constraint feasibility, and success rates, are detailed in Table I.

Inverse dynamics formulations achieved a significantly higher success rate compared to forward dynamics. For instance, in the double pendulum (`dpend`) system, the forward dynamics formulation struggled to converge and resulted in high feasibility errors. Conversely, inverse dynamics formulations not only achieved better constraint satisfaction with less iterations but did so even as the number of constraints increased. This is counterintuitive given its higher number of constraints compared to forward dynamics formulations.

D. Gymnastic maneuvers

As discussed in Section IV-B, our endpoint-explicit DDP algorithm successfully computed optimal trajectories for gymnastic maneuvers in the Talos humanoid robot. Despite the complexity and scale of these optimization problems, they are solved in fewer iterations, less seconds, and higher constraint

TABLE I
Average number of iterations for convergence, constraint feasibility, and success rate over 10 trials.

Problems	Iter.	Forward Dynamics		Inverse Dynamics		
		Feas.	Success	Iter.	Feas.	Success
qpose	14.5	2e-14	100%	15	2e-15	100%
bpose	23.9	6e-12	100%	24.3	2e-15	100%
dpend	7	4e+16	0%	46	1e-14	100%
bflip	126	1.3e-5	100%	107	6e-12	100%
fflip	236	3.9e-7	100%	218	5e-10	100%
mbar	48.7	15.47	0%	221.3	1.5e-3	60%
hstand	112.2	15.84	20%	69.3	2.70	50%

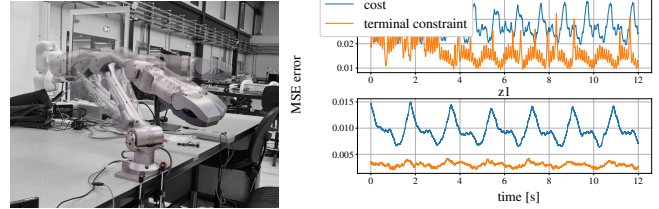


Fig. 4. Experiment trials with our endpoint-constrained MPC algorithm. (Left) Movements of the Z1 robot demonstrating. (Right) Tracking performance improvements in experimental trials with the B1-Z1 quadruped robot.

satisfaction than penalty-based approaches such as demonstrated in [16]. Fig. 1 showcases Talos performing gymnastic maneuvers, including a handstand, backflip, frontflip, and monkey bar.

E. MPC trials

To demonstrate the relevance of our endpoint-explicit method for control tasks, we conducted an experimental validation of our MPC controller. Our method was tested in two scenarios: a simulation involving the B1 quadruped equipped with the Z1 manipulator, and a real-world experiment on the Z1 manipulator, as depicted in Fig. 4 (left). Fig. 4 (right) compares the tracking error between the traditional cost-based penalty method and our approach, which incorporates a terminal constraint. In both scenarios, adding the terminal constraint led to improved tracking performance.

V. CONCLUSION

We introduced an exact method for handling endpoint constraints in differential dynamic programming, designed to efficiently tackle rank deficiencies. Our approach demonstrated high effectiveness across a wide range of optimal control problems, adeptly handling stagewise equality constraints like inverse dynamics and contact constraints. By reusing the Riccati recursion from problems without endpoint constraints, our method achieved exceptional computational efficiency, making it an ideal solution for real-time MPC in robotics. Looking ahead, we aim to extend this strategy to manage stagewise inequality constraints and unlock its full potential for parallelizing DDP algorithms.

REFERENCES

- [1] S. Boyd, N. Parikh, E. Chu, B. Peleato, and J. Eckstein, *Distributed Optimization and Statistical Learning via the Alternating Direction Method of Multipliers*, 2011.

- [2] A. L. Bishop, J. Z. Zhang, S. Gurumurthy, K. Tracy, and Z. Manchester, “ReLU-QP: A GPU-Accelerated Quadratic Programming Solver for Model-Predictive Control,” in *IEEE Int. Conf. Rob. Autom. (ICRA)*, 2024.
- [3] Y. Yang, X. Guan, Q.-S. Jia, L. Yu, B. Xu, and C. J. Spanos, “A Survey of ADMM Variants for Distributed Optimization: Problems, Algorithms and Features,” 2022.
- [4] F. Laine and C. Tomlin, “Parallelizing LQR Computation Through Endpoint-Explicit Riccati Recursion,” in *IEEE Conf. Dec. Contr. (CDC)*, 2019.
- [5] ———, “Efficient Computation of Feedback Control for Equality-Constrained LQR,” in *IEEE Int. Conf. Rob. Autom. (ICRA)*, 2019.
- [6] “Harwell Subroutine Library, AEA Technology, Harwell, Oxfordshire, England. A catalogue of subroutines,” <http://www.hsl.rl.ac.uk/>.
- [7] T. A. Howell, B. E. Jackson, and Z. Manchester, “ALTRO: A Fast Solver for Constrained Trajectory Optimization,” in *IEEE/RSJ Int. Conf. Intell. Rob. Sys. (IROS)*, 2019.
- [8] Y. Aoyama, G. Boutselis, A. Patel, and E. A. Theodorou, “Constrained Differential Dynamic Programming Revisited,” in *IEEE Int. Conf. Rob. Autom. (ICRA)*, 2021.
- [9] A. Pavlov, I. Shames, and C. Manzie, “Interior Point Differential Dynamic Programming,” *IEEE Trans. Contr. Sys. Tech. (TCST)*, vol. 29, 2021.
- [10] W. Jallet, A. Bambade, N. Mansard, and J. Carpentier, “Constrained Differential Dynamic Programming: A primal-dual augmented Lagrangian approach,” in *IEEE/RSJ Int. Conf. Intell. Rob. Sys. (IROS)*, 2022.
- [11] C. Mastalli, R. Budhiraja, W. Merkt, G. Saurel, B. Hammoud, M. Naveau, J. Carpentier, L. Righetti, S. Vijayakumar, and N. Mansard, “Crocoddyl: An Efficient and Versatile Framework for Multi-Contact Optimal Control,” in *IEEE Int. Conf. Rob. Autom. (ICRA)*, 2020.
- [12] J. Nocedal and S. Wright, *Numerical Optimization*, 2nd ed. New York, USA: Springer, 2006.
- [13] T. Rees and J. Scott, “A comparative study of null-space factorizations for sparse symmetric saddle point systems,” *Numerical Linear Algebra with Applications*, vol. 25, 2018.
- [14] N. Parikh and S. Boyd, “Proximal Algorithms,” *Found. Trends Optim.*, vol. 1, 2014.
- [15] P. E. Gill and D. P. Robinson, “A primal-dual augmented Lagrangian,” *Comput Optim Appl*, 2012.
- [16] C. Mastalli, S. Prasad Chhatoi, T. Corbères, S. Tonneau, and S. Vijayakumar, “Inverse-Dynamics MPC via Nullspace Resolution,” *IEEE Trans. Rob. (T-RO)*, vol. 39, 2023.
- [17] C. Mastalli, W. Merkt, G. Xin, J. Shim, M. Mistry, I. Havoutis, and S. Vijayakumar, “Agile Maneuvers in Legged Robots: a Predictive Control Approach,” 2022.
- [18] G. H. Golub and C. F. V. Loan, *Matrix computations*, 4th ed. The Johns Hopkins University Press, 2013.
- [19] Y. Tassa, T. Erez, and E. Todorov, “Synthesis and stabilization of complex behaviors through online trajectory optimization,” in *IEEE/RSJ Int. Conf. Intell. Rob. Sys. (IROS)*, 2012.
- [20] H. Li, W. Yu, T. Zhang, and P. M. Wensing, “A Unified Perspective on Multiple Shooting In Differential Dynamic Programming,” in *IEEE/RSJ Int. Conf. Intell. Rob. Sys. (IROS)*, 2023.
- [21] C. Mastalli, J. Martí-Saumell, W. Merkt, J. Sola, N. Mansard, and S. Vijayakumar, “A Feasibility-Driven Approach to Control-Limited DDP,” *Autom. Rob.*, 2022.
- [22] S. Martinez, R. Griffin, and C. Mastalli, “Multi-Contact Inertial Estimation and Localization in Legged Robots,” 2024.
- [23] H. Ferrolho, V. Ivan, W. Merkt, I. Havoutis, and S. Vijayakumar, “Inverse Dynamics vs. Forward Dynamics in Direct Transcription Formulations for Trajectory Optimization,” in *IEEE Int. Conf. Rob. Autom. (ICRA)*, 2021.